

DEVELOPMENT OF A YAG/OTR MONITOR FOR BEAM HALO DIAGNOSTICS*

R. Yang[†], P. Bambade, S. Wallon, LAL, CNRS/IN2P3, Université Paris-Saclay, Orsay, France
T. Naito, A. Aryshev, N. Terunuma, KEK, Tsukuba, Japan
M. Bergamaschi, CERN, Geneva, Switzerland

Abstract

To investigate the mechanisms of beam halo formation and its dynamics, a YAG/OTR monitor has been developed and tested at the KEK-ATF. The monitor has four ceramic Ce:YAG screens for the visualization of the beam core and beam halo and an OTR target to provide complementary beam core measurements. A high dynamic range ($>10^5$) and a high resolution ($<10\text{ }\mu\text{m}$) have been demonstrated experimentally. Measurements of beam halo using this monitor are consistent with previous results and theoretical modeling, and have allowed further progress in the characterization of the driving mechanisms.

INTRODUCTION

Beam halo is one of the critical issues limiting the performance and causing component damage and activation for the future linear or circular accelerator. Understanding halo formation and distribution is not only a crucial topic of accelerator physics but also of great importance for the mitigation of the unwanted background induced by halo particles, e.g., through an efficient collimation system. To uncover the physical origins of beam halo and how to suppress it, powerful diagnostics with extremely high dynamic range and sensitivity are required. Direct measurements of halo are considered for most accelerators, requiring a dynamic range of at least 10^5 and a capability to simultaneously measure core and halo, in order to appropriately probe theoretical predictions of beam halo [1–3].

As a successful test facility for the R&D of ILC, the Accelerator Test Facility (ATF) at KEK has provided an excellent opportunity to investigate the mechanisms of halo formation and demonstrate the necessary diagnostics [4, 5]. Its nominal beam energy and beam intensity are 1.3 GeV and $0.1 \times 10^{10} - 1 \times 10^{10}$ e/pulse, respectively. To achieve a sufficient dynamic range for halo measurements, a set of diamond sensor (DS) detectors have been developed and installed at ATF2 [6, 7], which is an extraction line built to address the feasibility of focusing electron beams to nanometer (nm) scale vertical size, and provide a beam orbit stability at the nm level at the virtual interaction point. After a reconstruction of measured profiles, the effective dynamic range of the DS detector has been found to be around 10^5 . Furthermore, the transverse beam profile and its vacuum dependence observed using these DS detectors clearly indicate the correlation between vertical beam halo and beam-gas scattering (BGS) [8]. However, the saturation of charge collection inside the DS bulk

and the deformations of DS waveforms have severely limited the performances and applications of the DS detectors [9]. To obtain a simultaneous diagnostics and confirm the observations given by the DS detector, a new YAG/OTR monitor has been developed and installed.

In this paper, the design of the YAG/OTR monitor toward the desired dynamic range and resolution are described, followed by performance tests with beam. Comparisons of beam halo measured by the DS detector and the YAG/OTR monitors are presented, which are in good agreement. Further foreseen applications and improvements of the YAG/OTR monitor are also discussed.

DEVICE CONFIGURATION

The favorable scintillating properties, mechanical rigidity and radiation hardness have made the scintillator material an excellent candidate for direct two-dimensional (2D) imaging devices, widely used for diagnostics of energetic particles and photons. Previous investigations have indicated that the Ce:YAG has a high photon yield (around 2×10^4 photons/MeV) and a fast decay time ($<1\text{ }\mu\text{s}$), which are suitable for halo diagnostics [10, 11]. Meanwhile, beam profile measurements using the OTR are saturation-free and can provide complementary diagnostics for dense beam core. Considering the practical beam parameters at ATF2, a YAG/OTR system has to satisfy two requirements: a dynamic range of more than 1×10^5 and a spatial resolution of less than $10\text{ }\mu\text{m}$.

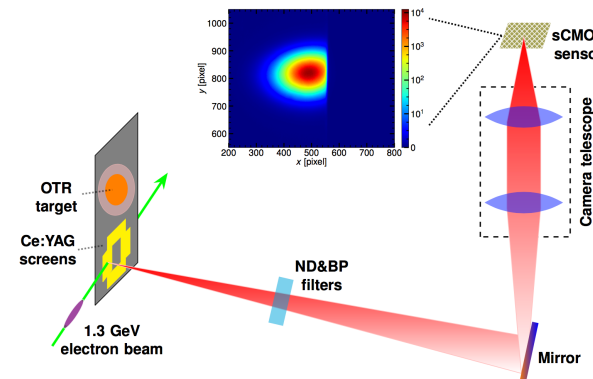


Figure 1: Schematic of the YAG/OTR monitor.

The YAG/OTR monitor mainly consists of four ceramic 0.5 mol% Ce:YAG screens and an OTR target on the same holder, a microscope lens (TS-93006/TS-93022 Sugito Co.), a 16-bit scientific Complementary Metal Oxide Semiconductor (sCMOS) camera (PCO.EDGE 4.2 L) with a low noise

* Work supported by MSCA-RISE E-JADE project (grant number 645479)
† ryang@lal.in2p3.fr

level and neutral-density (ND)/band-pass (BP) filters [12], as shown in Fig. 1. The scintillation light and OTR are extracted through a fused silica viewport with an indium seal to preserve a low vacuum pressure and then focused on the sCMOS sensor via an optical lens. To suppress the "blooming" effect due to the intense light from the beam core, a YAG screen has been split into four small pieces and assembled with a central quadrilateral opening ($4 \times 2.4 \text{ mm}^2$). The size of each YAG pad is $4 \times 5 \times 0.1 \text{ mm}^3$. For measurements of beam halo, the central opening allows core particles to pass through without striking the screen and emitting fluorescence light. Besides, an aluminum Kapton $2 \mu\text{m}$ thick OTR target has been seated in a titanium conical receptacle with an exposed screen diameter of 7 mm. The YAG screens are placed at 45° to the beam trajectory, and the observation is perpendicular to their surfaces, at 135° , horizontally. To probe the backward OTR with the same observation system, the OTR target is placed at 22.5° . In addition, a rectangular opening that is broader than the gap between YAG screens has been drilled on the holder in order to prevent the reflections from the surface of the holder (which has been found to blur the image significantly).

The holder to accommodate the screens is actuated by a four-dimensional manipulator (\vec{x} , \vec{y} , \vec{s} and the rotation around \vec{s} -axis). The backlash and readout accuracies of this manipulator have been calibrated to be around $13.5 \mu\text{m}$ and less than $0.2 \mu\text{m}$, respectively. To control the manipulator remotely, an interface has been developed in Python. Moreover, two dedicated softwares have been developed for data acquisition and adjustment of the camera position along with attached optical objective.

DYNAMIC RANGE

The lower limit of the dynamic range is mainly determined by the photon yield (PhY) of the YAG screen, the photon collection efficiency and the background noise level. On the other hand, the upper limit is related to the scintillation saturation, which can in principle be corrected by using also the OTR to image the dense beam core. The 0.5 mol% ceramic Ce:YAG manufactured by Konoshima Chemical Company, Ltd., Japan has been used [13]. The scintillating light spectrum is centered near 525 nm with a transparency above 80%, and the PhY has been measured to be about 2×10^4 photon/MeV. The energy deposition inside the YAG has been evaluated to be around 0.1 MeV/e based on the ESTAR stopping power database [14], and through a Monte Carlo simulation with the MCNPX code [15]. Then, the photon emission efficiency can be further estimated to be about 2000–2500 photon/e. Assuming the scintillation light is mainly in a range from 500 nm to 600 nm, the transmission of light through the viewport and the optical lenses is around 85% and the effective observation angle is 6.2 mrad for a magnification factor of 3, the photon collection efficiency is expected to be about 0.32–0.4 photon/e. Notice that the reduction of the observation angle due to the refraction of the exiting scintillation light has been taken into account [16].

The sCMOS camera is placed at 30 mm above the beam line in order to suppress the background from upstream. However, the background noise from the sCMOS sensor is unavoidable and is relevant to the temperature of the sensor (10°C thanks to the cooling system), the shutter mode and the exposure time. In rolling shutter mode, measurements exhibit a non-uniform distribution of pixel noise level and rms background noise less than 1 digital count for an exposure time of 10 ms, as shown in Fig. 2. One may notice that the readout has a constant offset which has been designed to ensure a low readout noise. For the absolute readout versus the number of incident photons, such an offset can be determined experimentally and then subtracted. After removing this offset, the residual readout noise/deviation is about 0.5 count/pixel, which is corresponding to 0.33 photon/pixel taking into account a quantum efficiency of 70% and a A/D conversion of 0.46 e/count.

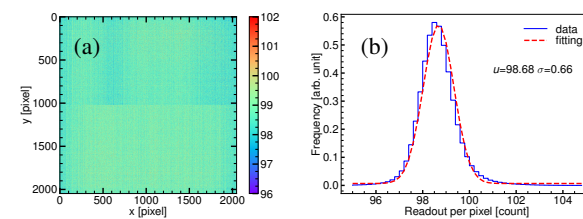


Figure 2: Background image (a) and its histogram (b).

To ensure reliable detection of halo particles, a signal-to-noise of more than three is necessary. Following this, the minimum number of incident photon per pixel should be larger than one, which means a minimum particle density of four electrons over one-pixel size on the YAG screen.

The maximum particle density without scintillation saturation depends on the concentration of Ce ions and can be analytically estimated as

$$\rho_{e,\max} = \frac{\rho_{Ce}}{\beta n_{eh} E_d} \quad (1)$$

where ρ_{Ce} is the density of the doped Ce ions, β the transport efficiency, n_{eh} the density of produced e-h pair and E_d the energy deposition. An upper limit for the saturation threshold is calculated as $100 \text{ fC}/\mu\text{m}^2$. However, it has to be confirmed through experimental measurements. Focusing the beam vertically using a quadrupole (QD20) upstream, the saturation threshold could be extrapolated from the maximum particle density on the YAG screen when the total photon collection/production begins to decrease. For a beam intensity of $3 \times 10^9 \text{ e/pulse}$, the flux of YAG scintillation light tends to be constant (1.2×10^9) when the beams are large enough and then the photon collection reduces when focusing the beam down to $40 \mu\text{m}$, as shown in Fig. 3. During the transition from saturation-free to saturation, a lower limit for the saturation threshold was found to be $16\text{--}18 \text{ fC}/\mu\text{m}^2$.

Furthermore, for a magnification factor of 2.5, the effective particle density is estimated to be $4\text{--}4.8 \times 10^5 \text{ e/pixel}$ in the absence of scintillation saturation. The maximum

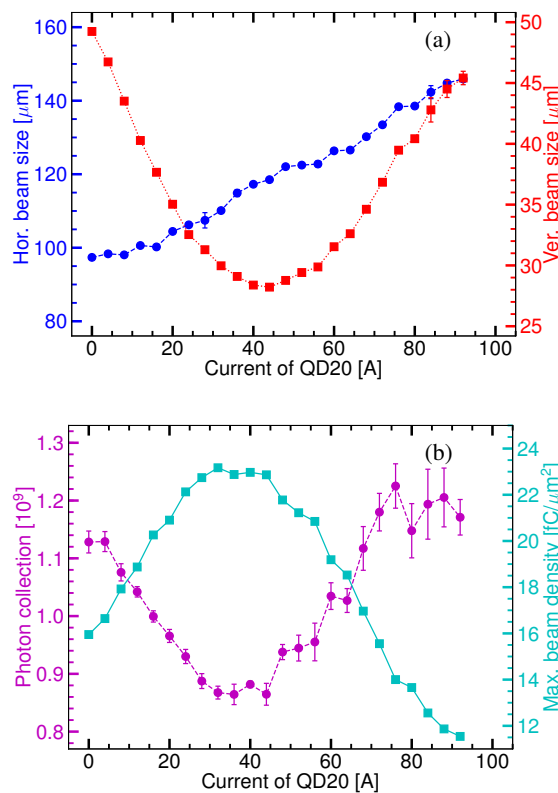


Figure 3: Vertical and horizontal beam sizes (a) and the number of incident photons on the camera sensor (b) as a function of the QD20 current.

readout of the measured 2D beam profiles is about 2×10^5 , which also indicates an effective dynamic range of about 1×10^5 , as shown in Fig. 4. Moreover, the dynamic range can be further extended by combining the images from OTR screen (core) and YAG screens (halo) with a valid algorithm.

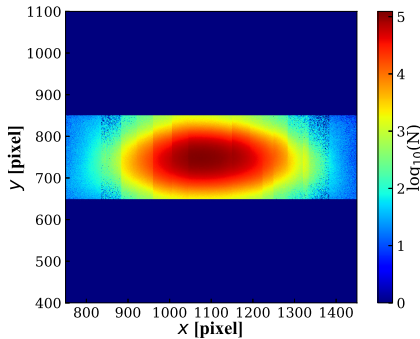


Figure 4: 2D beam profile without scintillation saturation measured by YAG screens.

SPATIAL RESOLUTION

The nominal vertical and horizontal beam sizes at the YAG/OTR monitor are less than 30 μm and more than

6. Transverse profiles and emittance monitors

100 μm, respectively. To avoid the scintillation saturation, the vertical beam size is normally enlarged, e.g., to be larger than 50 μm, using the QD20 quadrupole. The spatial resolution of the YAG screen is mainly determined by the optical diffraction limitation, the finite thickness of the screen, the pixel size and the saturation effect. Without the scintillation saturation, the vertical resolution is given by

$$\sigma_{\text{res},y} = \sqrt{\sigma_{\text{diff}}^2 + \sigma_f^2 + \sigma_{\text{px}}^2} \quad (2)$$

where σ_{diff} is the resolution associated to the optical diffraction, σ_f the resolution related to the thickness of the scintillator and σ_{px} the pixel size. Assuming a magnification factor of 3, the vertical resolution is estimated to be about 2.08 μm. The horizontal resolution is however degraded by the overlap of scintillation light emitted from different depths. Numerical simulations suggest that the measured beams sizes are significantly larger than what they should be only when the real beam sizes decrease to below 50 μm and 100 μm, vertically and horizontally, respectively. On the other hand, the resolution for measurements using the OTR screen is mainly determined by the optical diffraction and can be characterized by the rms of the point spread function [17]. For the light in the 450–700 nm range, the resolution for OTR measurements is found to be around 5.4–8.4 μm.

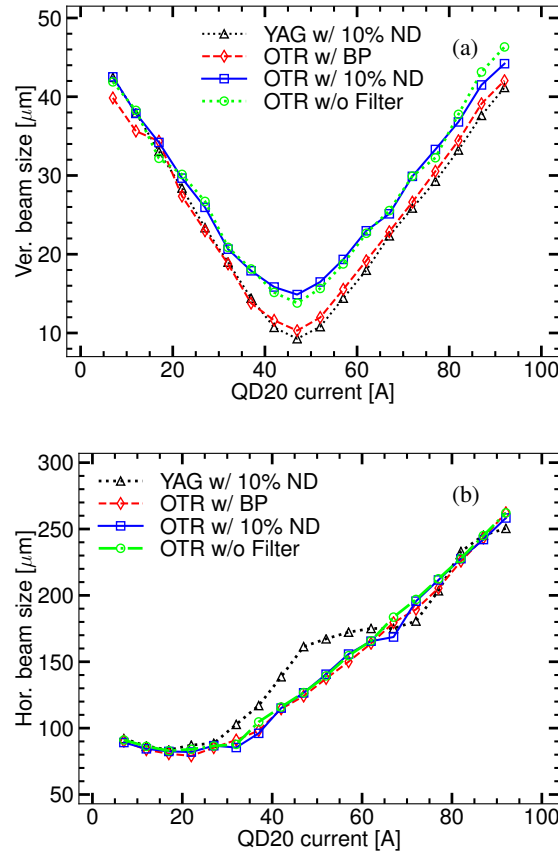


Figure 5: Evolution of vertical (a) and horizontal (b) beam size as a function of QD20 current.

Focusing the beam with the QD20 quadrupole, the minimum vertical beam size has been found to be around $9.3\text{ }\mu\text{m}$ using the YAG screen, with either a 10% ND filter or a $550\pm10\text{ nm}$ BP filter, and about $10.2\text{ }\mu\text{m}$ from the OTR image with the same BP filter, as shown in Fig. 5 (a). Besides, enlargement of the horizontal beam size measured by the YAG screen due to the scintillation saturation was clearly observed when the vertical beam size was smaller than $25\text{ }\mu\text{m}$, as shown in Fig. 5 (b). From these measurements, we could conclude that the resolution of the YAG/OTR monitor is below $10\text{ }\mu\text{m}$, vertically, and accomplishes our design goals.

HALO MEASUREMENTS

Considering the configuration of four YAG pads, measurements of the vertical or horizontal distributions are performed in the following way. Taking the vertical case as an example, the holder is firstly adjusted to obtain an image of the bottom halo particles, where the scintillation light is weak and the influence from the beam core is negligible. Then, part of the image below a "boundary", which is about $50\text{--}100\text{ }\mu\text{m}$ beneath the edge of the YAG pad, is recorded as an effective slice of the whole beam profile. Subsequently, the bottom YAG pad is moved up to get images of more halo particles. A new "boundary" is then determined, and the part between the previous and new "boundaries" is taken and combined with the existing slices. Repeat such process until entering the core region where the 10% or 1% ND filters will be inserted to attenuate the light intensity and then one moves to the top YAG pad to acquire the upper half profile. The full beam profile is eventually assembled by integrating all the slices after subtracting a common background noise/offset. The reconstructed 2D beam distribution indicates a dynamic range of 1×10^5 , as shown in Fig. 4. However, the projection of the obtained 2D profile is only valid along the scanning direction.

Halo measurements were performed for various vacuum pressures of the damping ring and compared with the theoretical predictions in the presence of BGS. Good agreement between measurements and predictions are observed for the vertical beam halo but not the horizontal one, as shown in Fig. 6. They are consistent with the measurements using the DS detector, and further confirm the previous experimental observations and the conclusion that the vertical beam halo is dominated by the BGS process.

CONCLUSION

A high dynamic-range YAG/OTR monitor has been designed and constructed for precise beam halo diagnostics at ATF2. This monitor consists of four ceramic 0.5 mol% Ce:YAG screens and an OTR target on a holder, and an observation system. The analytical and experimental evaluations have suggested that the background noise is less than one photon per pixel, and a lower limit of the scintillation saturation threshold is about $16\text{--}18\text{ fC}/\mu\text{m}^2$. The effective dynamic range for 2D beam profiles measured using the YAG screens has been demonstrated to be more than 1×10^5 ,

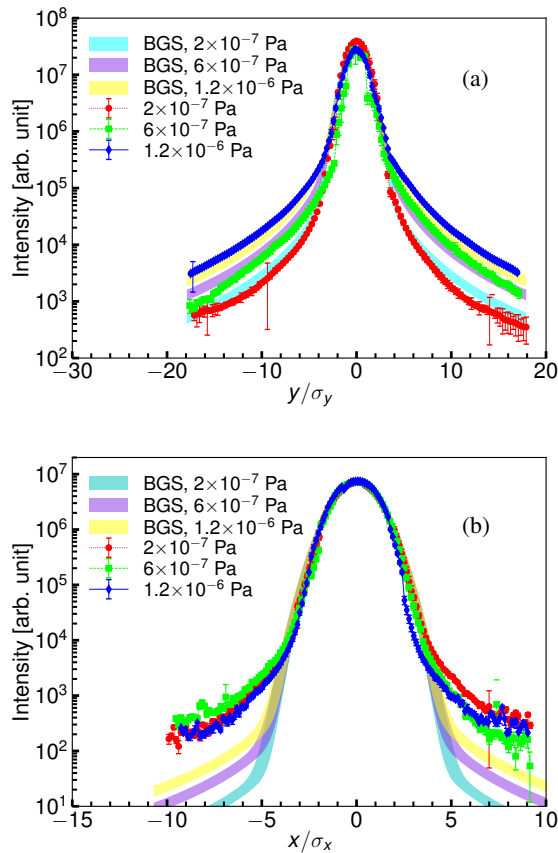


Figure 6: Vertical (a) and horizontal (b) beam profiles measured by YAG screens. Notice that the distributions are normalized to rms beam sizes in order to compare with the theoretical predictions.

which is sufficient for beam halo studies. Besides, the spatial resolution of this monitor is less than $10\text{ }\mu\text{m}$ for both the YAG screen and OTR target, satisfying our the design goals.

Measurements of vertical and horizontal beam halo for different vacuum pressures of the damping ring have been performed following a dedicated profile scanning method, and are found to be consistent with previous observations. Furthermore, to extend the dynamic range of the YAG/OTR monitor, the combination of images from the YAG screens and OTR is under investigation.

ACKNOWLEDGEMENTS

The authors would like to express their gratitude to the ATF collaboration and to the staff and engineers of ATF. We wish to thank T. Lefèvre for the support of the sCMOS camera and Z. Hu for his help with the MCNPX simulation.

REFERENCES

- [1] K. Wittenburg, "Beam halo and bunch purity monitoring," *CERN Accelerator School 2009-005*, pp. 557–580, 2009.
- [2] T. Mitsuhashi, "Beam halo observation by coronagraph," in *Proc. 7th European Workshop on Beam Diagnostics and In-*

- strumentation for Particle Accelerators (DIPAC2005)*, Lyon, France, Jun. 2005, paper ITMM03, pp. 7–11.
- [3] H. D. Zhang *et al.*, "Beam halo imaging with a digital optical mask," *Phys. Rev. ST Accel. Beams* 15(7): 072803, 2012.
- [4] K. Kubo *et al.*, "Extremely low vertical-emittance beam in the Accelerator Test Facility at KEK," *Phy. Rev. Lett* 88(9): 194801, 2002.
- [5] G. R. White *et al.*, "Experimental validation of a novel compact focusing scheme for future energy-frontier linear lepton colliders," *Phy. Rev. Lett.* 112(3): 034802, 2014.
- [6] B. Grishanov *et al.*, "ATF2 proposal," 2005.
- [7] S. Liu *et al.*, "In vacuum diamond sensor scanner for beam halo measurements in the beam line at the KEK Accelerator Test Facility," *Nucl. Instrum. Meth. A* 832 (2016): 231–242.
- [8] R. Yang *et al.*, "Evaluation of beam halo from beam-gas scattering at the KEK Accelerator Test Facility," *Phys. Rev. Accel. and Beams* 21(5): 051001, 2018.
- [9] R. Yang, "Diagnostics and characterization of beam halo at the KEK Accelerator Test Facility," Ph.D. thesis, Université Paris-Saclay, Orsay, France, 2018.
- [10] M. Moszyński *et al.*, "Properties of the YAG: Ce scintillator," *Nucl. Instrum. Meth. A* 345(3): 461-467, 1994.
- [11] T. Naito and T. Mitsuhashi, "Beam halo measurement utilizing YAG: Ce screen," in *Proc. 4th International Beam Instrumentation Conference (IBIC2015)*, Melbourne, Australia, Sep. 2015, pp. 373–376.
- [12] <https://www.pco.de/scmos-cameras/pcoedge-42/>
- [13] T. Yanagida *et al.*, "Evaluation of properties of YAG (Ce) ceramic scintillators," *IEEE transactions on nuclear science*, 52(5): 1836–1841, 2005.
- [14] M.J. Berger, "ESTAR, PSTAR, and ASTAR: Computer programs for calculating stopping-power and range tables for electrons, protons, and helium ions," 1992.
- [15] L. S. Waters, "MCNPX user's manual," Los Alamos National Laboratory, 2002.
- [16] A. Murokh *et al.*, "Limitations on the resolution of YAG: CE beam profile monitor for high brightness electron beam," *The Physics of High Brightness Beams*, pp. 564–580, 2000. https://doi.org/10.1142/9789812792181_0038
- [17] P. Karataev *et al.*, "First Observation of the Point Spread Function of Optical Transition Radiation", *Phy. Rev. Lett.* 107(17): 174801, 2011.